OPEN ACCESS

University of BRISTOL

Peer reviewed version

Link to published version (if available):
10.1016/j.polymer.2016.02.002

Link to publication record in Explore Bristol Research
PDF-document

Morphing nacelle inlet lip with pneumatic actuators and a flexible nano composite sandwich panel

Nazli Gulsine Ozdemir[1], Fabrizio Scarpa[1], Monica Craciun[2], Chrystel Remillat[1], Cristian Lira[3], Yogesh Jagessur[1], Luiz Da Rocha-Schmidt[4]

[1] Advanced Composites Centre for Innovation and Science (ACCIS), University of Bristol, BS8 1TR, Bristol, United Kingdom

[2]Centre for Graphene Science, University of Exeter, EX4 4QL, Exeter, United Kingdom

[3]National composites centre (NCC), BS16 7FS, Bristol, United Kingdom

[4]Technische Universität München, Institut für Luft und Raumfahrt Lehrstuhl für Leichtbau, Boltzmannstr. 15 D-85748 Garching, München, Germany

Abstract

We present a hybrid pneumatic/flexible sandwich structure with thermoplastic nanocomposite skins to enable the morphing of a nacelle inlet lip. The design consists of pneumatic inflatables as actuators and a flexible sandwich panel that morphs under variable pressure combinations to adapt different flight conditions and save fuel. The sandwich panel forms the outer layer of the nacelle inlet lip. It is lightweight, compliant and impact resistant with no discontinuities, and consists of graphene-doped thermoplastic polyurethane (G/ TPU) skins that are supported by an aluminium Flex-core honeycomb in the middle, with near zero in-plane Poisson's ratio behaviour. A test rig for a reduced-scale demonstrator was designed and built to test the prototype of morphing nacelle with custom-made pneumatic actuators. The output force and the deflections of the experimental demonstrator are verified with the internal pressures of the actuators varying from 0 to 0.41 MPa. The results show the feasibility and promise of the hybrid inflatable/nanocomposite sandwich panel for morphing nacelle airframes.

Keywords

Morphing nacelle; pneumatic actuation; flexible sandwich panel; graphene toughened thermoplastic polyurethane; nanocomposite; lightning strike protection

1. Introduction

Morphing technologies are targeted to improve the flight performance and broaden the flight envelope of aircraft by enabling shape change during flight [1]. In the recent years, various morphing technologies have been proposed, mainly consisting of flexible structures. An example is NextGen's morphing wing structure made from silicone skin with stiffening ribs that provide out of plane stiffness, while allowing necessary shear deformations [2, 3]. In a similar way, Chen et al. have embedded pneumatic muscle fibres under a morphing skin with a silicone rubber matrix and has evaluated the morphing capability of this configuration [4]. Chen et al. also introduced a novel composite flexible skin with in-plane negative Poisson's ratio behaviour to tailor the actuation force necessary for morphing and the synclastic curvature of the composite [5]. In the field of inflatable structures, Sun et al. presented an active honeycomb structure with tubular inflatable systems and an auxetic cellular structure for morphing wingtip applications [6]. In another active morphing work, Sun et al. sandwiched flexible tubes between two custom honeycomb layouts where the air foil thickness was increased when the tubes in the prototype demonstrator were inflated [7]. Pneumatic artificial muscles (PAMs) known for their lightweight and high output have demonstrated high potential for inflatable actuation in aerospace applications [8]. Woods et al. have looked into the cyclic loading characteristics of PAMs and significantly extended the fatigue life of these inflatable structures simply by modifying their design [9].

Morphing skins have similar deformation mechanisms to the ones present in human skin, in which the embedded curved fibrils re-orientate towards the tensile direction and resist the load only when stretched to their full length. The same fibrils provide out of plane stiffness to

the skin [10]. Olympio et al. have also demonstrated that the curved strands embedded inside a flexible rubbery skin reduce the residual strains and the required morphing actuation force [11].

Adaptive morphing structures such as NASA's adaptive compliant wing (FlexFoil) require structures that need to be lightweight and flexible, but also resistant to high aerodynamic pressures at the same time [12]. The key criteria is to design a structure that provides a low in-plane stiffness to reduce the energy consumption of the actuators, but at the same time possess sufficient stiffness to maintain the aerodynamic configuration during the deformation process. With these in mind, a candidate solution would be flexible sandwich panels with rubbery skins and a compliant cellular honeycomb core [13, 14]. Cellular structures are lightweight materials that provide out of plane stiffness through transverse shear, which are widely used in aerospace applications [15, 16]. Honeycombs with near zero in plane Poisson's ratio (ZPR) and negative Poisson's ratio (auxetic) are more suitable for complex cylindrical applications than the conventional cores that attain positive internal cell angles [17]. Such conventional honeycombs generate anticlastic curvature (saddle shape) when subject to out of plane bending [18, 19]. Hexcel's patent Flex core honeycomb maintains a near ZPR behaviour for large cell sizes, and it is already being used in aerospace industry.

Flexible thermoplastics (TPs) have been employed as constituents for smooth continuous morphing skins [13, 4, 11, 20]. They show a high potential for the future aircraft technologies, and smart structures composed of these materials could offer short cycle times of operations, recyclability, ability to re-process the material and lower cost of manufacturing. Flexible TPs can bear high deformations but also need to withstand high aerodynamic pressures. The latter performance target could be achieved by supporting the flexible skins with a compliant flexible core, like a Flex core aluminium honeycomb. For morphing structures on the outer surface of the aircraft the materials used need to offer

multifunctional capabilities by showing moderate electrical conductivity to mitigate critical electrostatic build-up for possible lightning strike discharge [21]. In this work we propose a flexible graphene doped thermoplastic polyurethane skin that has less electrical resistivity and a higher bending and compressive modulus at an extremely low graphene level.

Graphene possesses high potential as polymer reinforcement for its exceptional properties of electron transport, mechanical toughening and high surface area [22, 23]. Recently, scalable production of large quantities of defect free graphene has been developed [24], for the potential commercialisation of graphene in aerospace industry. However, dispersion of graphene inside thermoplastic matrices can be quite difficult because of the high viscosities that these matrices attain, and this area needs to be explored further [25]. Thermoplastic polyurethanes (TPUs) are block copolymers comprising of hard and soft segments. Their special chemical structure makes them versatile, with excellent tear and abrasion resistance, high compression and tensile strength, and they are operable at wide range of temperatures. In this regard, their properties can be tailored through the inclusion of nanofillers to their structure [26, 27].

This study introduces novel flexible sandwich panels with graphene doped TPU skins that sandwich a Flex core aluminium honeycomb. To the best of the Authors' knowledge, a flexible sandwich panel with TPU skins that offers high out of plane and low in plane stiffness has not been proposed before and it may represent an alternative structural design solution for morphing aircraft technologies in nacelle engine applications. Aero engine nacelles form the outer, aerodynamically smooth covering for a jet engine to reduce noise and fuel consumption. The airflow through the nacelle inlet lip can be tailored for noise and thermodynamic engine performance by introducing morphing capabilities, requiring the shape changing structures to withstand aerodynamic pressures in the range of 89 KPa – 100 KPa, and convergent-divergent inlet channel configurations through inflatable systems with

actuating pressures of the order of 0.05 MPa to 0.40 MPa [28, 29]. We introduce to this extend a morphing structural concept demonstrator made by an adaptive flexible sandwich panel with TPU/graphene skins and embedded pneumatic actuators underneath. The pneumatic actuators are inflated to create various pressure contours, and an aerodynamically optimal shape could therefore be achieved. Small-scale prototypes have been produced and tested under mechanical 3-point bending tests. A custom test rig representing the inflatable system has also been designed and built, and used to evaluate the morphing capability of the flexible structure for different combinations of inflatable pressure configurations.

2. Morphing nacelle inlet lip concept

Within the scope of the EU project "MorphElle" [28], a novel nacelle lip-morphing concept was developed. The project partners Bauhaus Luftfahrt, Germany, and Kungliga Tekniska Högskolan, Sweden cover the operational and aerodynamic parts of the design respectively, while the authors' focus lies on the structural and materials aspects of the project. To realise the concepts introduced herein, the nacelle inlet lip should exhibit a sufficient stiffness to maintain the shape under aerodynamic loads, however at the same time it needs to show compliance for the shape morphing capability. The skin also needs to have a smooth surface to decrease drag and it needs to be electrically conductive for lightning strike protection. To achieve these goals, thermoplastic polyurethane was doped with graphene and flexible skins with and without graphene dispersion have been produced for comparison. Flexible sandwich panels comprising of the TPU and G/ TPU skins have been manufactured by introducing a novel compression moulding technique. The small-scale prototype demonstrator of the morphing nacelle inlet lip concept consists of two inflatable bladders beneath the flexible sandwich panel. The bladders are inflated to different pressures to achieve various aerodynamic contours for the convergent-divergent duct shape morphing configurations

(Figure 1). By achieving specific pressure contours during flight, the inlet lip (highlighted red in Figure 1) provides a smooth airflow change through the nacelle duct.
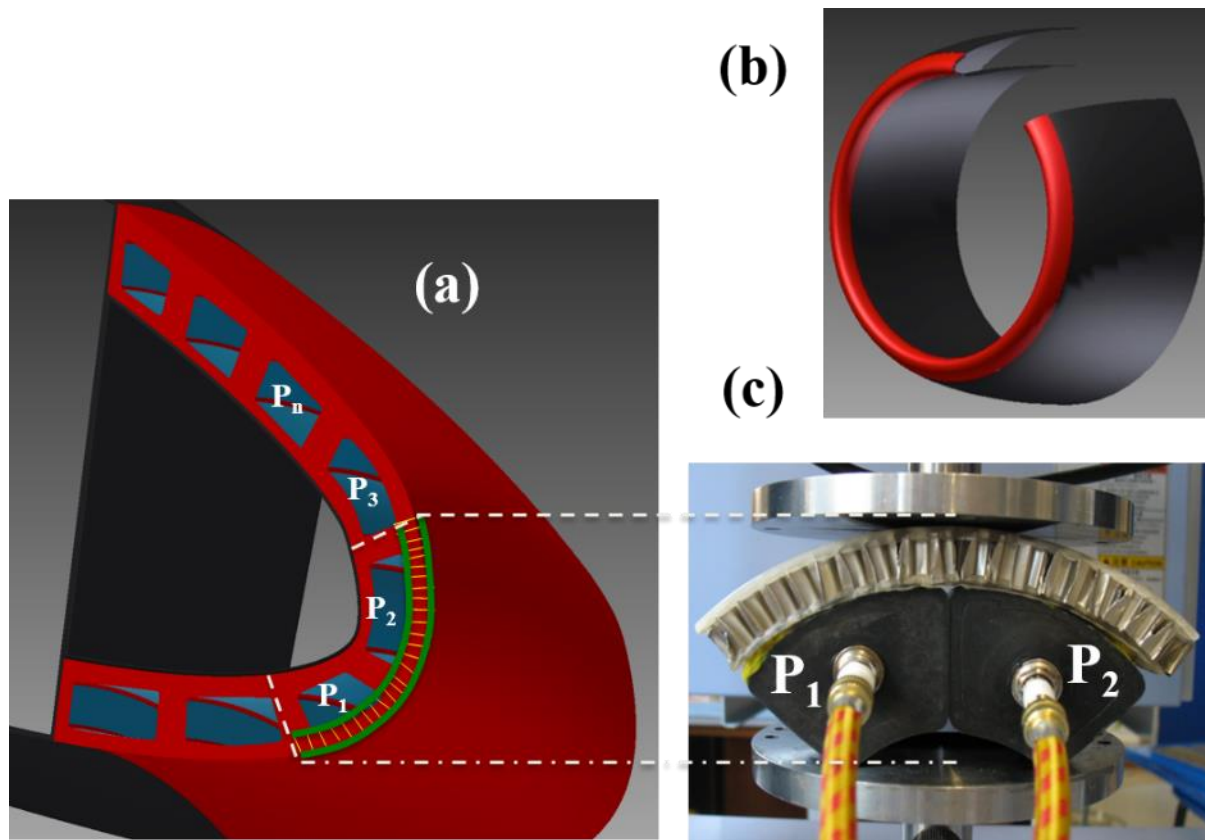

Figure 1. (a) Inventor model of the morphing nacelle inlet lip concept [29, 28], **(b)** Inlet lip region highlighted red in a nacelle [29, 28], **(c)** Prototype demonstrator of the nacelle inlet lip with a flexible sandwich panel and embedded pneumatic actuators

3. Materials and manufacturing

The flexible sandwich panel consists of an aluminium honeycomb (Flex core 5052 F40-.0013, Hexcel UK) with anisotropic properties (in-plane Poisson's ratios v_{12}=0.9 and v_{21}=0.5, and Young's Moduli E_1=0.4 MPa and E_2=0.2 MPa. Flex core's specific properties contrast with honeycombs with regular hexagons that attain in-plane Poisson's ratios of +1, and an out of plane Poisson's ratio nearly of 0 (v_{13}) [30]. Flex core honeycombs can be easily bent into a convex shape. The skins have been produced out of TPU pellets (Estane 58271, durometer hardness value 86A) that were compression-moulded in custom-made steel

moulds (Figure 2). Prior to manufacturing, the pellets were dried in a vacuum oven at 80°C for 5 hours to remove any water content. A spray able release agent (Lusin Alro OL151) was applied on the moulds and left to dry for 15 minutes. Fifty and sixty grams of TPU pellets were placed in the lower and upper skin mould cavities respectively (Figure 2). The moulds with the pellets were then heated up to 200°C in the press and left for 30 min to stabilise the temperature. The pellets were pressed at a pressure of 2 MPa for half an hour using an electrically heated hydraulic compression press, after which the pressure was reduced and the moulds were left to cool at RT. The aluminium Flex-core was cut to size with a steel blade and the surfaces in contact with the TPU skins were sanded with a fine sand paper. The Flex-core was cleaned with acetone and dried at room temperature for 15 minutes. Cilbond 48 adhesive (Chemical Innovations ltd. UK) was applied on the surfaces with a brush and the aluminium core was left to dry for 30 min. The Flex-core was then placed between the TPU skins inside the mould. The temperature of the press was set to 120°C to enable the softening of the skins and to allow 1.5 mm of the thin walled aluminium core to penetrate through the softened skins at a pressure of 1.2 MPa on each side. These conditions were maintained for 3 hours. The mould was then allowed to cool down to room temperature (RT) (23°C), and then the flexible sandwich panel was taken out.

Figure 2. (a) Custom-made steel moulds of the upper and the lower face skins, filled with TPU pellets prior to compression moulding, **(b)** Flexible sandwich panels, left: with TPU skin, right: with graphene doped thermoplastic polyurethane (G/ TPU) skin

The parameters defining the flexible sandwich panel and the Flex core honeycomb unit cell are detailed in Figure 3 and Table 1. In the current design, a thickness of 1.5 mm of Flex core penetrates into the 3 mm thick TPU face skins on each side, creating honeycomb reinforced thermoplastic skins that offer high bending stiffness. Moreover, the depth necessary to achieve the same bending stiffness in conventional honeycombs is reduced [31]. Similarly, the adhesion between the skins and the core is significantly improved as the flexible panel

creates at the interface a monolithic single structure that guarantees a strong bonding and continuity of displacements under the large deformations required for a shape changing structure, something that the common use of thin layer adhesives in composite structures to apply actuators for morphing may not be able to provide [32].
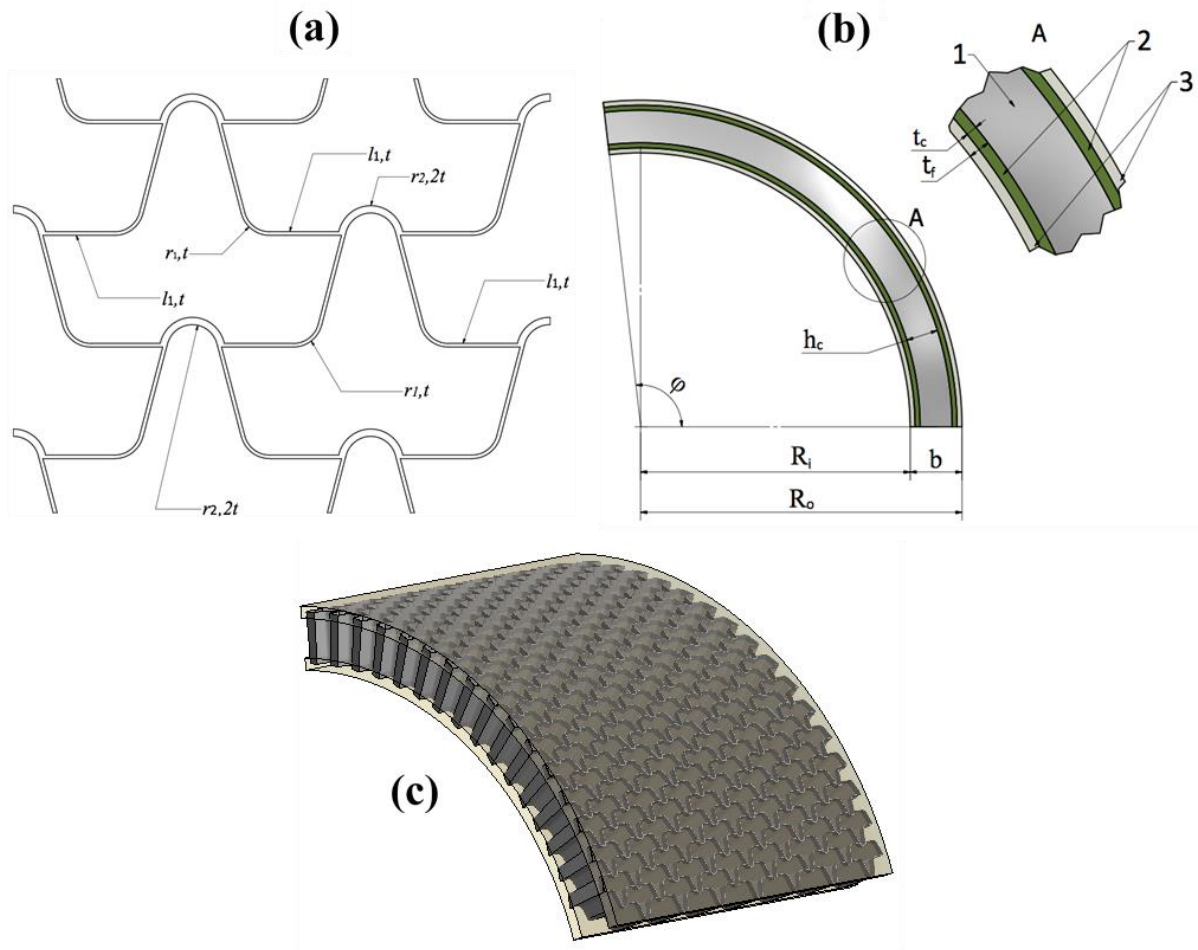

Figure 3. Geometry parameters defining **(a)** The Flex core honeycomb unit cells, **(b)** Dimensions of the curved sandwich panel, **(c)** 3D Inventor model of the curved sandwich panel

Table 1. Parameters of the curved sandwich panel and the Flex core honeycomb, σ_c (compression strength) in MPa, ρ (density) in g/ cm^3, the other units are in mm

Curved sandwich panel		Flex core unit cells	
1	Aluminium Flex core honeycomb	l_1	2.50
2	Al Flex core reinforced TPU composite	l_2	3.38
3	TPU face skins	t	0.06
R$_O$	97.30	σ_c	1.55
R$_i$	81.60	d	0.08
b	15.70		
t$_c$	1.50		
t$_f$	3.00		
h$_c$	9.70		
φ	96.70°		

3.1 Test rig design and manufacturing

Compared to the full scale morphing lip (Figure 1), the test rig design is simplified in terms of complexity to keep the development and preliminary design costs down while still demonstrating the desired morphing capabilities. The number of pressure chambers is reduced to two, which is the minimal number to show a significant shape morphing. Using reinforcement directions as illustrated in Figure 4, enables the circumferential strains that occur during the lip movement.
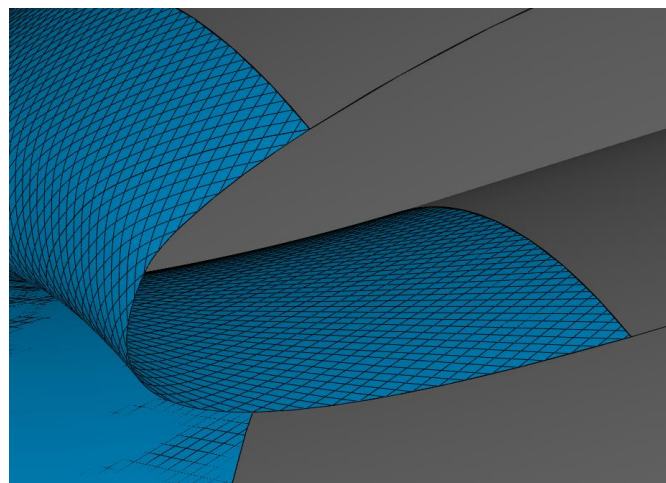
Figure 4. Reinforcement orientation of the nacelle lip

It is assumed that the external aerodynamic forces will be known from CFD analyses for each flight condition and the internal actuation pressures are to be interpreted as differential pressures between the external aerodynamic loading and the pressure generated by the internal pneumatic actuation.

Custom-made inflatable actuators (Indico rubber, UK) from nylon reinforced natural rubber of 4 mm wall thickness were placed underneath the curved sandwich panel, as shown in Figure 5. A pressure regulator (Airgas, 0-1.38 MPa) controlled the pressure inside the inflatables. A 3D printed ABS stand with 100% filling ratio supported the inflatables to impose the main actuation force on the flexible sandwich panel by trapping the inactive sides.

In the real scenario, this entrapment will be achieved by the inflatables themselves, pushing towards each other when inflated. The curved sandwich panel enclosing the inflatables and the ABS stand were contained by a thin steel metal mesh (Spoerl, Germany) with an aperture size of 0.8 mm and yield strength of 1.1 N/m. The metal mesh was clamped on each side underneath the ABS stand with the help of two custom made steel clamps. The metal mesh provides a highly compliant skin effect due to the $\pm$ 45° layout of the metal wires working in in-plane shear under out-of-plane deformation of the structure underneath [29].
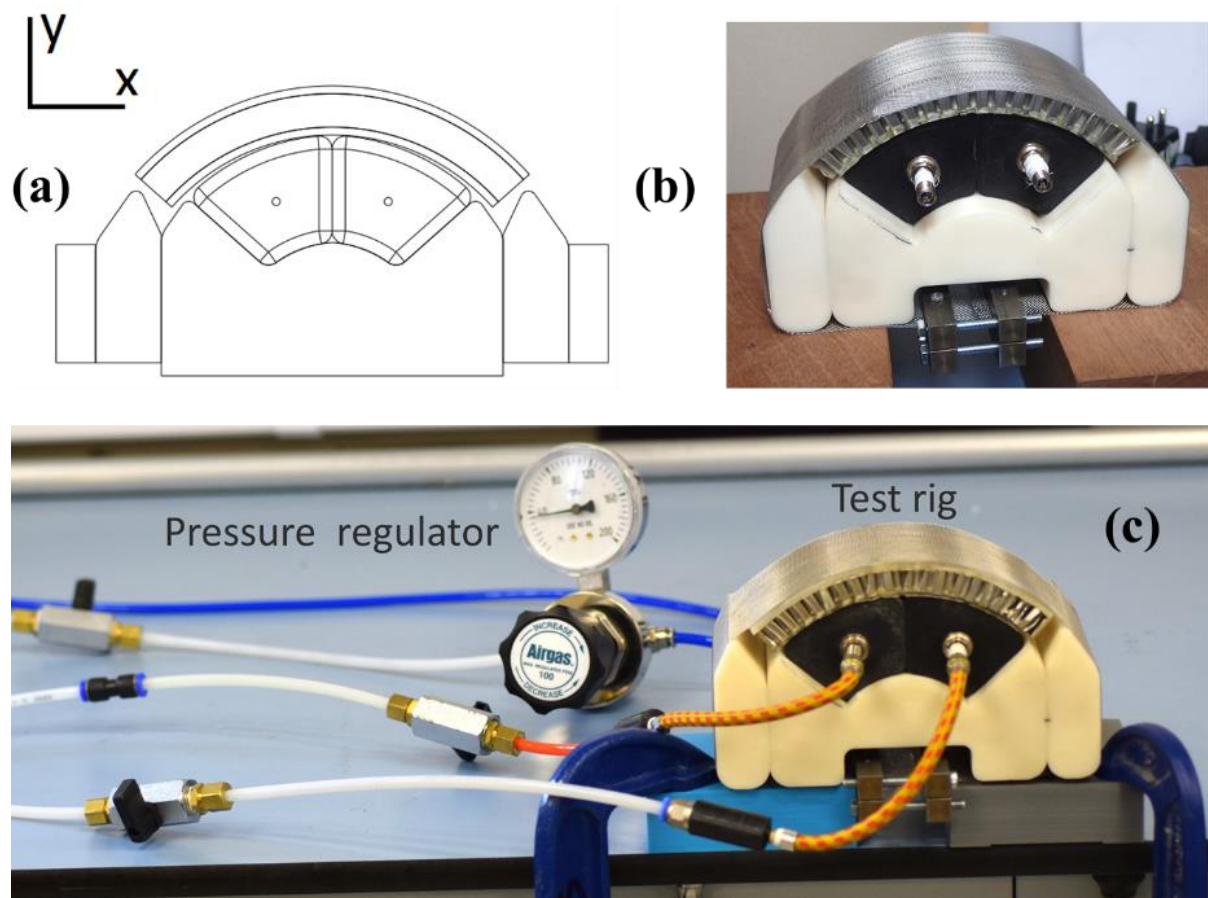

Figure 5. Prototype test rig for the inflatable actuation, **(a)** Inventor model of the test rig with the coordinate axis, **(b)** Test rig, **(c)** The prototype demonstrator for the nacelle inlet lip

3.2 Face skins manufacturing

Graphene / water solution

A solution comprising 600 ml of water, 1 g graphite powder (<20μm), synthetic, 0.02 g sodium cholate hydrate bioxtra, ≥99%, (both supplied from Sigma Aldrich, UK) was high shear mixed with a Silverson L5M machine at 5000 rpm for 3 hours. The final solution gives a graphene (G) concentration of ~0.17 wt%. The solution was then drop casted on a silicon wafer (100 mm N<100> as doped, single side polished, IDB Technologies ltd.) that was placed on a hot plate at 150°. After drying the wafer was cleaned with acetone to wash away the sodium cholate hydrate. The drop casted wafer surface was inspected with a Jeol Field Emission Gun scanning electronic microscope (SEM) 6330 at secondary electron (SE) mode. Figures 7 (a) and (b) show some square-shaped multi layers of graphene as recorded from the SEM analysis. It is interesting to note that the graphene layers are similar in size, with a ~300X300 nm surface area and also feature sharp edges. From the observation of Figure 7 (b) it can also be noticed that few layers of graphene sheets are stacked on the top of each other. A Renishaw Raman spectroscope (using 532 nm wavelength excitation and a 100x objective lens) was used to further confirm the presence of graphene in the solution. In Figure 7 (e), a clear G band (~1580 cm^{-1}) is noticeable, which is related to the E_{2g} vibrational mode of graphene. The 2D band (~2700 cm^{-1}) is also used to identify graphene and the presence of the D band (~1350 cm^{-1}) is related to the density of the defects in graphene, mostly derived from the edge effects [33].

Graphene / thermoplastic polyurethane (G/ TPU) skins

To fabricate the skins 240 grams of TPU pellets were added into 1000 ml of G/ water, and the solution was ultrasonicated for 1 hour at room temperature (23°C) at on-off mode and amplitude of 40% to avoid overheating. TPU pellets were left in the G /water dispersion overnight, after which they were filtered and dried in a vacuum oven at 80°C for 5 hours and

left in a desiccator prior to compression moulding. The G/ TPU pellets were further analysed with the Renishaw Raman spectroscope. For this analysis a single pellet was placed under the microscope and the laser beam was focussed on the surface. In Figure 7 (e), the presence of characteristic G and 2D bands is evident in the Raman spectra of the pellet (G/ TPU sample), meaning that the graphene remains bonded to the surface of the pellets. It is interesting to notice that the 2D band shifted to the right in the close-up Raman spectra of the G/ TPU pellet (Figure 8), and the main reason for this type of shift is attributed to stress fields [34]. There is also a small shift in the G band from 1574 to 1578 cm^{-1}. It is possible that stress transfer takes place as the graphene layers are bonded on the surface of the TPU pellets in the water solution [35]. Stress transfer from the TPU pellets to the graphene can also be monitored from the shift of the 2D and the G Raman band.

For the compression moulding of the graphene-coated pellets a spray-able release agent (Alro OL 151 Chem Trend) was applied to the steel moulds and left to dry for 15 minutes. The G/ TPU pellets were placed inside the mould cavities and the temperature was left to stabilise at 180°C after which the moulds were closed and the pellets were pressed at 2 MPa for 30 minutes (Figure 2 (a)). The moulds were then left to cool at room temperature after which the face skins were demoulded with the help of the ejector pins. For cyclic compression testing, cylindrical disks (Figure 6) were moulded in custom-made steel cylindrical cavities at the same pressing conditions. A random piece from the G/ TPU disk was cut and conditioned with distilled water at room temperature. The cured nanocomposite was coated with silver for the analysis with a FEG SEM. Figures 7 (c) and (d) show the fracture surface of the G/ TPU sample. It can be seen that the graphene platelets are stacked on the top of each other, displaying some aggregation in the cured sample. The electrical conductivity of the samples was determined following the ASTM D4496-04 standard. For this, a high resistance meter with a two-point probe was used and resistivity measurements were performed on five

samples. The samples were pre-treated following the guidelines of the ASTM D6054 standard, with copper wires bonded to each side of the specimens with a conductive epoxy adhesive (Circuitworks, CW2400), and the adhesive was then cured in an oven at 150°C for 10 minutes. The resistivity of the samples was measured after a period of 60 seconds, which is known as the electrification time. The resistivity (R) was calculated through the slope of I-V curves with Ohm's law.
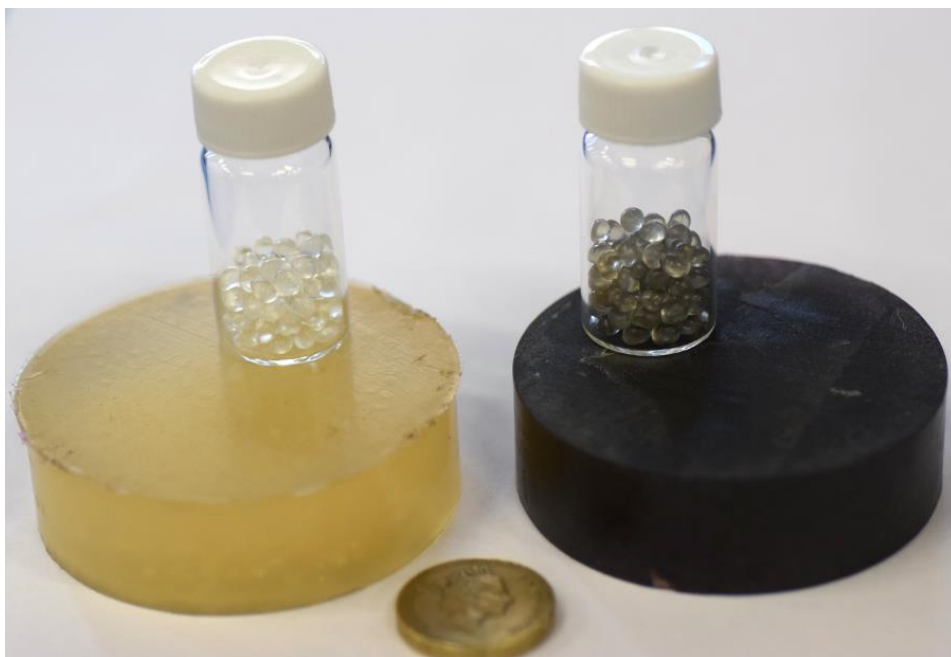

Figure 6. Cylindrical disks, TPU (left) and G/ TPU (right) formulations
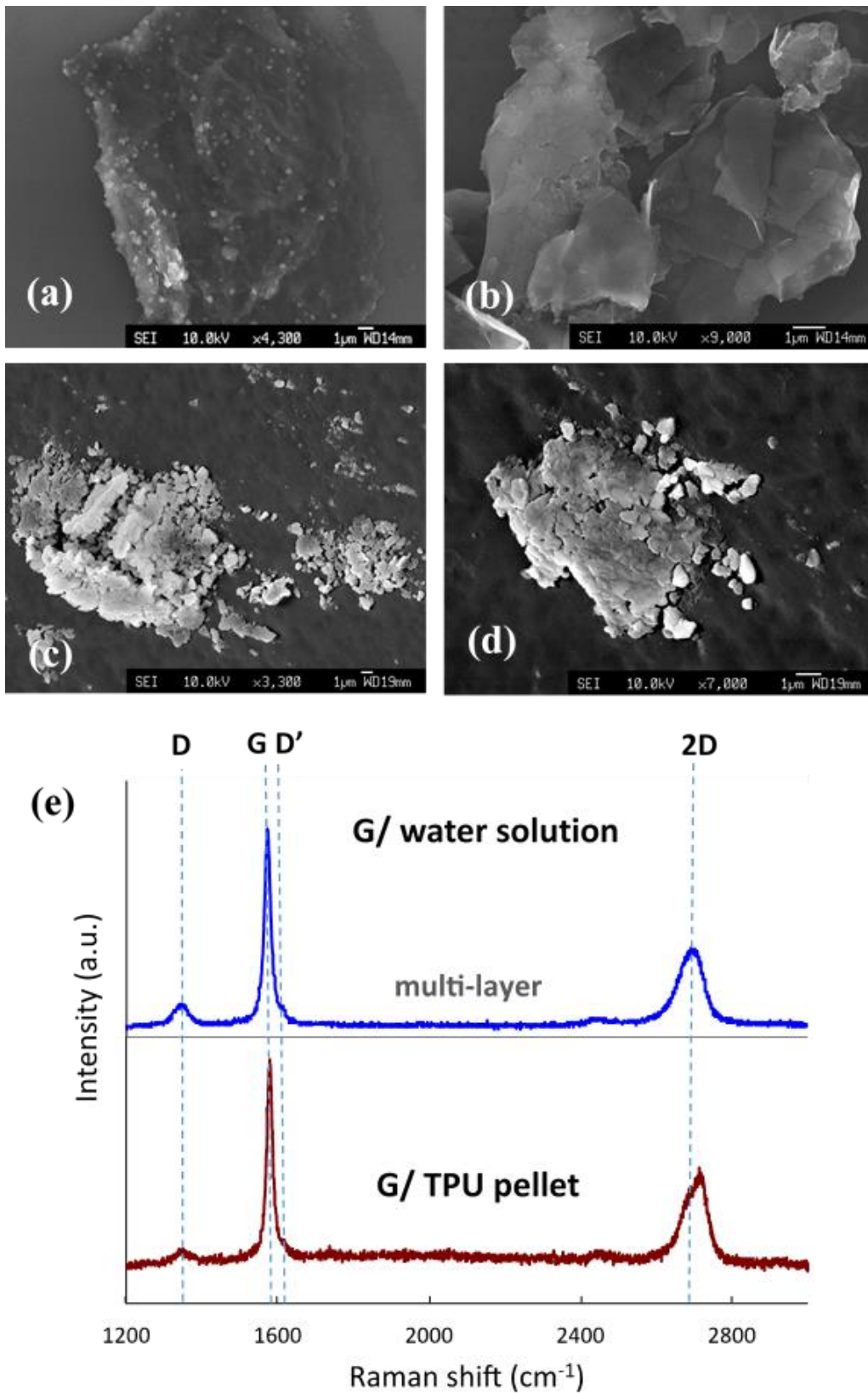
Figure 7. (a), (b) FEG SEM image of the drop casted G/ water solution on the silicon wafer,

(c), (d) FEG SEM image of the fracture surfaces of the cured G/ TPU sample, **(e)** Raman

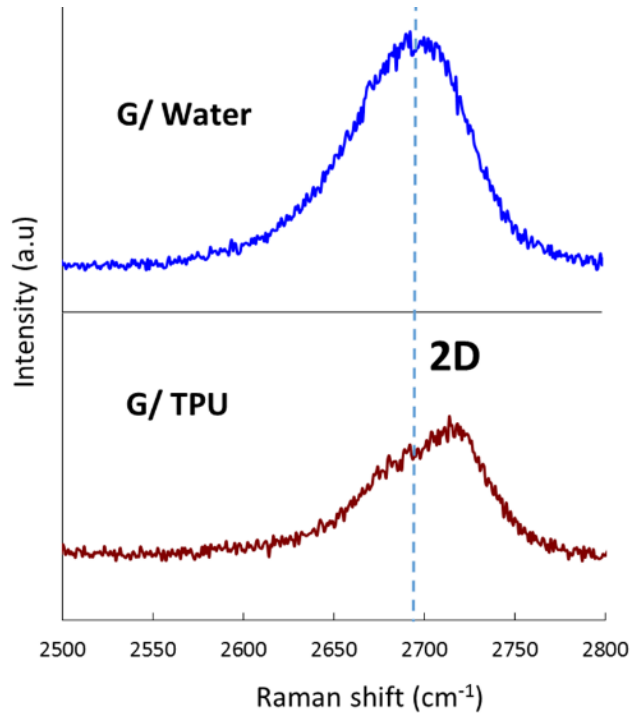spectra of the G/ water solution and the surface of the TPU pellets coated with graphene

Figure 8. Close-up Raman spectra of the G/ water solution and the surface of the TPU pellets coated with graphene

Cyclic compression tests

Cyclic compression tests were performed to quantify parameters such as elastic modulus, hysteresis, time dependent loading effects, loss factor and cyclic softening. For this, cylindrical disks with dimensions of H=20 mm and D=65 mm were tested under compression loading using a tensile machine (Shimadzu AGS-X, maximum force 10 kN, Shimadzu Corp., Kyoto, Japan). The samples were subjected to 20 loading-unloading cycles at a crosshead rate of 2 mm/min. The loss factor was calculated for each complete loading-unloading cycle with the following equation:

$$\delta = \frac{\Delta W}{W} \tag{1}$$

Where ΔW is the dissipated energy that corresponds to the area inside the hysteresis and W is the total work calculated from the integration of the area under the initial loading curve.

Figure 9 (a) shows the compression load-deflection graphs of the samples. The compressive elastic modulus of the cylindrical disks was calculated at 10% deflection. The maximum force detected from each cycle vs. the cycle number n is plotted in Figure 9 (b). Here, the maximum force value tends to stabilise after a few cycles, with most softening occurring during the initial few cycles. The stiffness loss after 20 cycles is around 5.7 % for the pure TPU samples and lower (4.5 %) when the graphene is used as doping of the TPU pellets. It can also be observed that the decay in the maximum force value is higher in the G/ TPU samples (597 N) when compared to the TPU sample (414 N). This may be attributed to the breaking of the attachments between the hard graphene filler and the soft TPU chains, hence a higher amount of softening [36]. Table 2 gives the compressive strength (σ_c) data calculated in accordance with ASTM D 1621-00, indicating a 10% improvement with 0.17 wt.% of graphene addition to the TPU. The compressive stiffness was also improved by 11% from 2.26×10^6 to 2.52×10^6 N/m. This significant increase in the stiffness with only 0.17 wt. % of graphene addition may be a result of the rubber-filler attachment restricting the movement of the chains in the cross-linked network. Large gains in stiffness have been previously reported in open literature, particularly with polyurethane matrices [37, 38]. The increase in modulus was attributed to the large difference in stiffness between the filler and the matrix, as illustrated by Halpin-Tsai bounds [39]. There is also possibility that the graphene interacts with the soft polyurethane segments through van der Waals interactions, making more difficult the motion of the chains [38].

The manufacturing process for the graphene doped TPU matrices proposed herein is simple and environmentally friendly. The process does not necessitate the usage of expensive solvents such as the ones currently being used in literature for exfoliation of graphite (THF and NMP) [27, 24], and it is compatible with large-scale industrial processes. Table 2 also indicates a higher electrical conductivity proving that the graphene doped thermoplastic

polyurethane is moderately conductive. Such conductivity is insufficient to provide lightning strike protection to the skins, but shows the high promise of graphene as a dopant to tailor the mechanical and the electrical properties of thermoplastic matrices. In this study, the graphene doped TPU skins will serve as a vehicle to carry the electrical charge through the aluminium Flex core. The conductivity value is in good agreement with the literature for similar weight ratios of graphene dispersion [40, 41]. The loss factor remained constant, which means that the dissipated energy did not show a noticeable variance over the number of cycles.
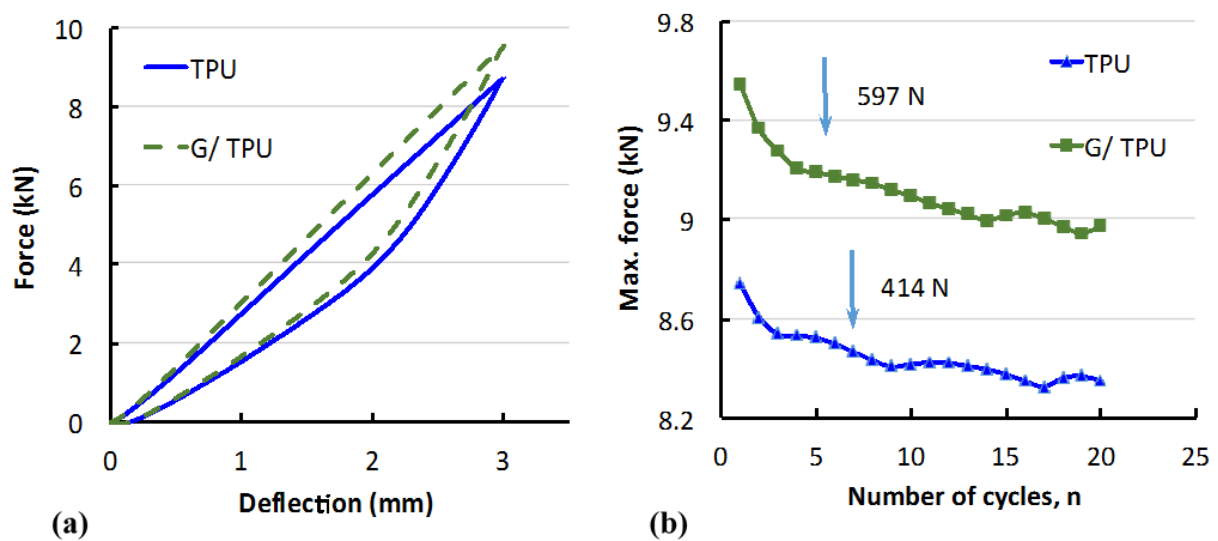
Figure 9. **(a)** Compression tests on the samples at a rate of 2 mm/min, **(b)** Maximum load (kN) vs. number of cycles, n

Table 2. Properties of the cylindrical disk samples, E (N/m): compressive stiffness

Sample	σ_c (MPa)	E (N/m)	Loss factor	Electrical conductivity (S/m)
TPU	1.71	2.26×10^6	0.27	1.00×10^{-13}
G/ TPU	1.88	2.52×10^6	0.27	1.87×10^{-9}

The sandwich panels were subjected to three-point bending loading at a loading speed of 2 mm/min using a tensile machine (Shimadzu AGS-X, maximum force 10 kN, Shimadzu Corp., Kyoto, Japan). The load was applied on the samples until a 100% radial deformation was achieved, following unloading until the sandwich panel recovered its initial shape. The bending stiffness of the sandwich panels was calculated at 10% of radial deformation extracted from the initial loading curve. From Figure 10 it is evident that the flexible panel with the G/ TPU skins withstands higher loads at the same crosshead deflections due to the higher stiffness of its nanocomposite skins. A 20% improvement in the bending modulus of the flexible panels is achieved with only 0.17 wt% of graphene dispersion (Table 3), showing that graphene may constitute a solution to tailor the mechanical properties for morphing applications, while at the same time offering a moderate electrical conductivity. Quite interestingly, the loss factor for the flexible sandwich panels with G/ TPU skins is significantly higher (0.37) when compared to the panels with TPU skins (0.23). It is likely that the improved bonding provided by the G/TPU skins in contact with the Flex core honeycomb contributes to the dissipation of more strain energy during the cyclic loading, and therefore leads to a higher hysteresis inside the loading-unloading cycle.

Table 3. Properties of the flexible curved sandwich panels

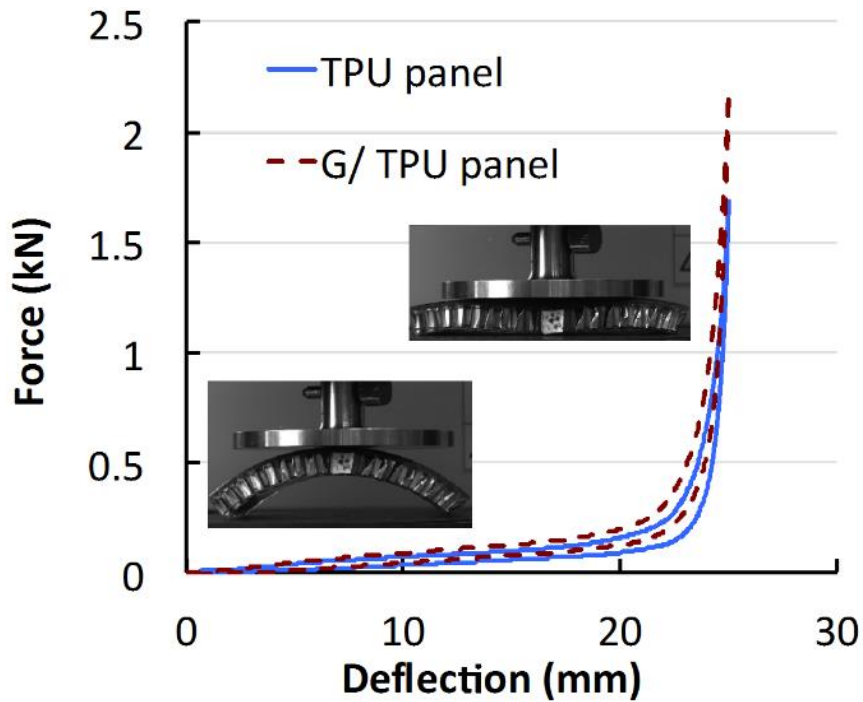| Panel skin	Bending stiffness (N/m)	Loss factor
TPU	6768	0.23
G/ TPU	8150	0.37

Figure 10. Force vs. displacement graphs of the sandwich panels tested under three-point bending load at a crosshead speed of 2 mm/min

4. Morphing performance

The actuation force of the demonstrator was investigated by creating various pressure contours and exposing it to cyclic compression loading. The prototype morphing nacelle lip was subjected to compressive central point loading using a tensile machine (Shimadzu AGS-X, maximum force 1 kN, Shimadzu Corp., Kyoto, Japan) at a crosshead speed of 1 mm/min. The force-displacement diagrams of the morphing prototype for $P_1=P_2=0$ MPa and $P_1=P_2=0.0345$ MPa are shown in Figures 11 (a) and (b) respectively. The force-controlled experiments were repeated for 3 times. In Figure 11 (b), it is assumed that the bladders are inflated to a pressure of 0.0345 MPa to retain a defined shape under external pressure contours. Figure 11 (b) shows a good level of repeatability whereas in Figure 11 (a) the force decreased consistently from the initial (1st) to the last (3rd) experiment, due to the contraction of the experimental prototype. Hence, it is necessary that the actuators are inflated to a

minimum pressure to retain a constant shape during flight under external aerodynamic pressures.
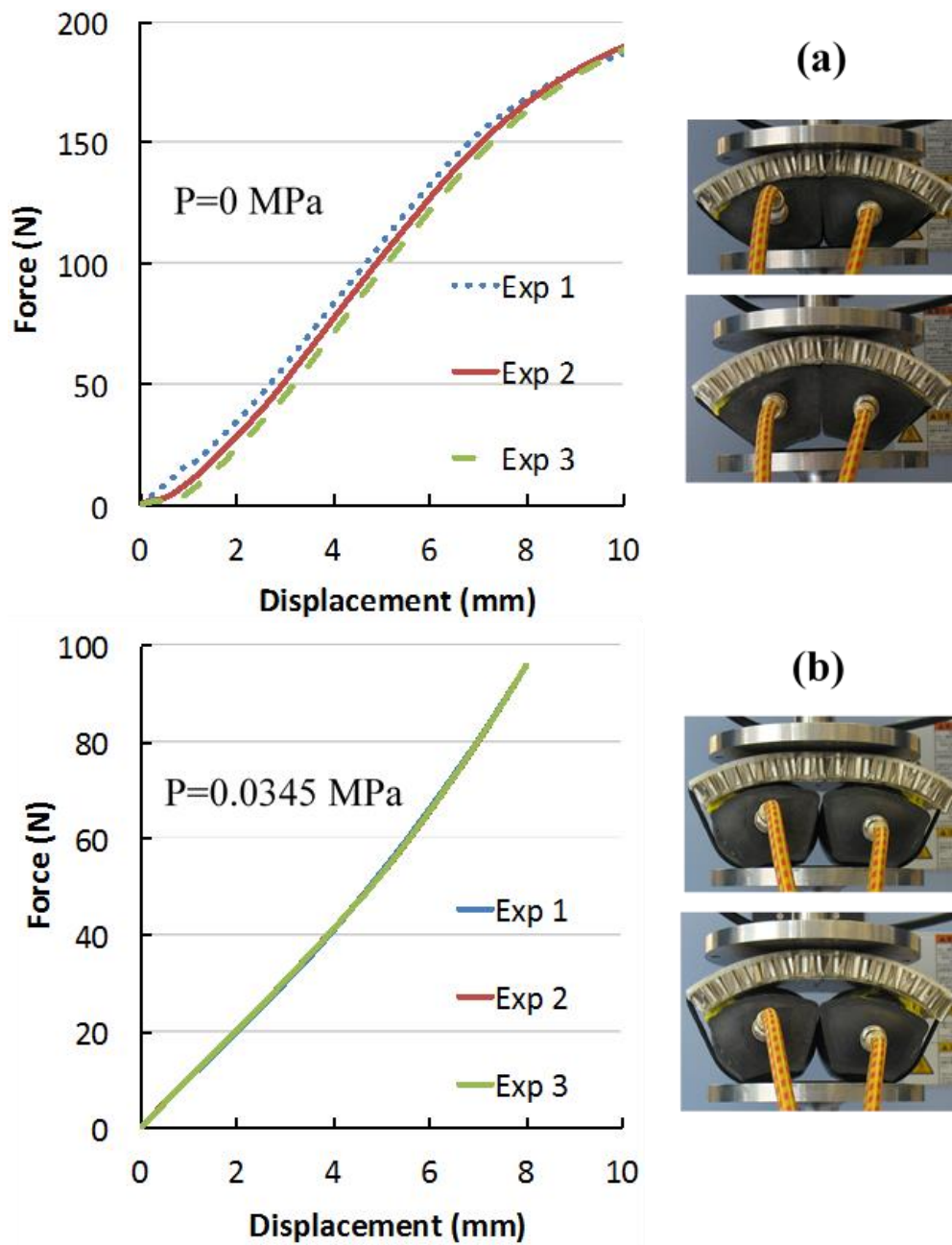

Figure 11. Force vs. displacement in compression test, **(a)** $P_1=P_2=0$ MPa, **(b)** $P_1=P_2=0.0345$ MPa (5 PSI)

Figure 12 shows the force exerted on the crosshead vs. the pressure P_1, where $P_1=P_2$ at different crosshead displacements s (mm). At each imposed displacement the force was zeroed before starting the experiment. A quasi linear relationship between the inflatables' pressure and the output force can be observed at every crosshead displacement for pressures above 0.06 MPa.
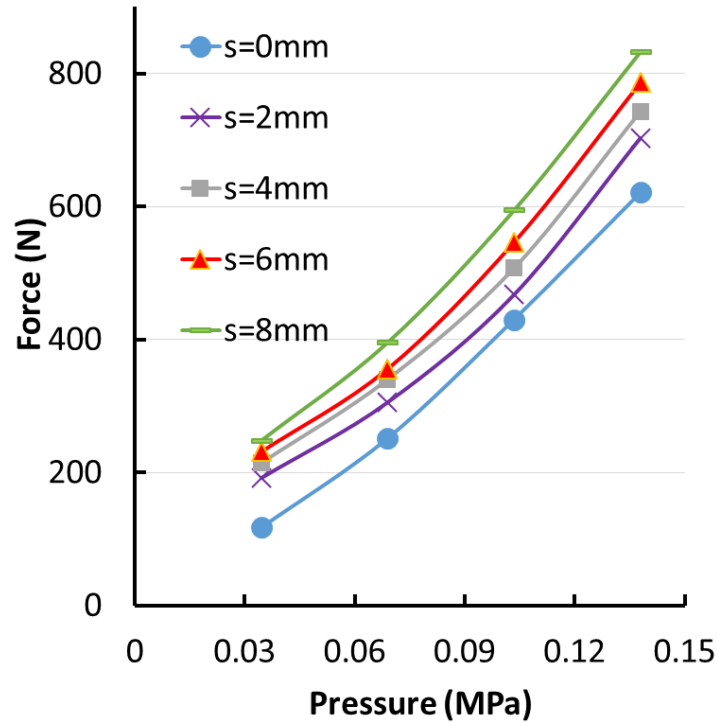
Figure 12. Output force vs. input pressure ($P_1=P_2$) for different crosshead displacements, s

5. Evidence of morphing capability

The morphing capability of the flexible sandwich structure was evaluated with the custom test rig. A one camera (Imetrum non contact precision measurement) and a two camera video gage (Dantec Dynamics digital 3D Image correlation system Q400) were installed to track the displacement of the target points. The two-camera system enabled tracking of the proper deflection of the curved area whereas the one camera system tracked the y-direction deflection of the target points only. The test rig setup for the 2 cameras system is shown in Figure 13.

Figure 13. Test rig setup for 2-camera video gage system

Figures 14 and 15 give the graphs that represent the shapes of the sandwich panels corresponding to the sets of experiments conducted with the one camera video gage system. In Figure 14, a mirror image is attained when the pressure contours were (0.0 MPa, 0.07 MPa) and (0.07 MPa, 0.0 MPa), and a maximum y-direction deflection of 6% was achieved. (The coordinates are indicated in Figure 5). This initial experiment proves that the actuation force imposed by the inflatables is similar and the curvature can be precisely controlled.
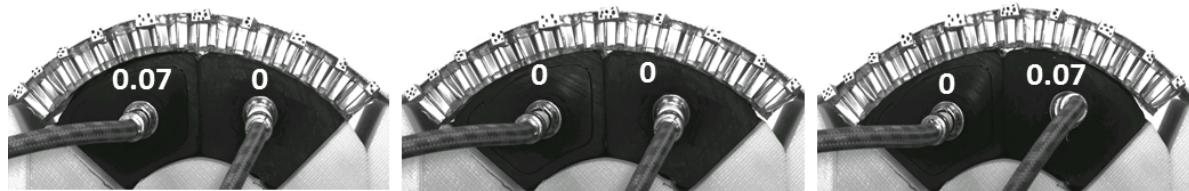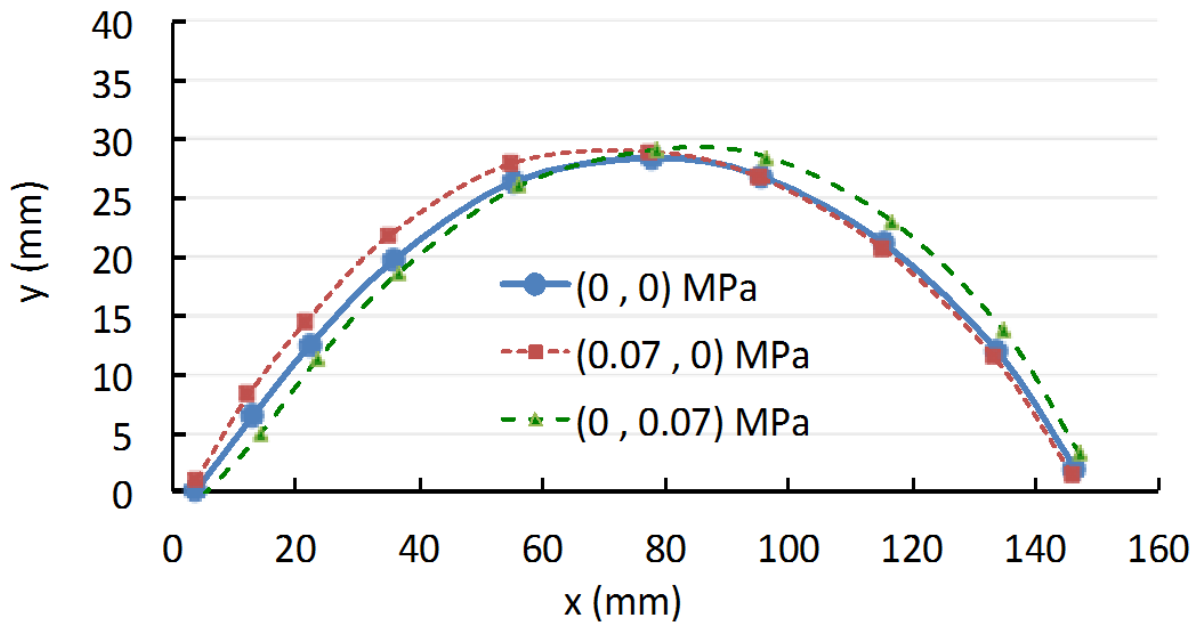
Figure 14. Shape morphing at configurations of (0.07 MPa, 0.0 MPa), (0.0 MPa, 0.0 MPa) and (0.0 MPa, 0.07 MPa)

Another set of experiments was done to further evaluate the morphing capability of the system. All sets of experiments started from the initial configuration (0.07 MPa, 0.07 MPa), and then further inflation was created setting the pressures to (0.41 MPa, 0.07 MPa). The sandwich panel achieved a maximum of 19% deflection along the y-direction (Figure 15 (b)). A smooth and consistent camber variation was generated at every pressure contour. It is worth noticing that the initial (0.07 MPa, 0.07 MPa) configuration needs to be kept all times to maintain a constant shape and prevent any undesirable shape changes resulting from the contraction of the inflatables. Figure 16 shows the % deflection along the y direction vs. the maximum pressure when one of the inflatables was inflated to a higher pressure. It is worth noticing the linearity of the response (similar to the one shown in the unconstrained rig layout of Figure 11). Quite importantly, the data show that the response of the morphing panel does

not change with the equal pressures combinations ((P_1=c, P_2=b) or (P_1=b, P_2=c)). This is a clear indication of the quality of the manufacturing and base design used for the fabrication of the demonstrator.
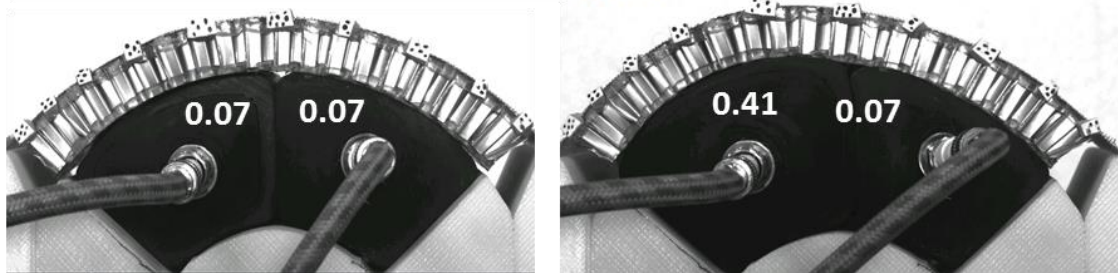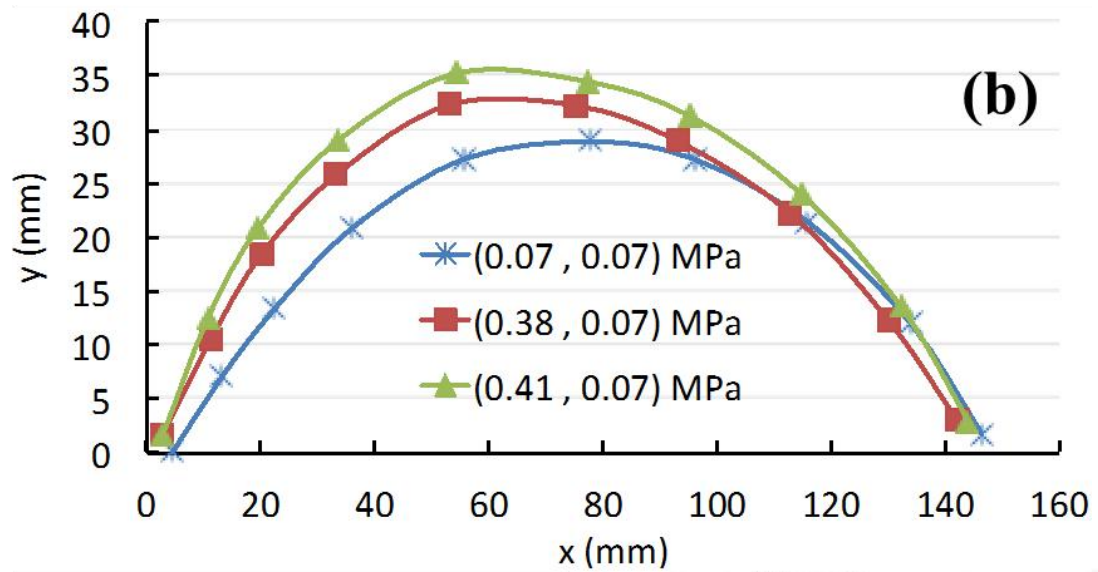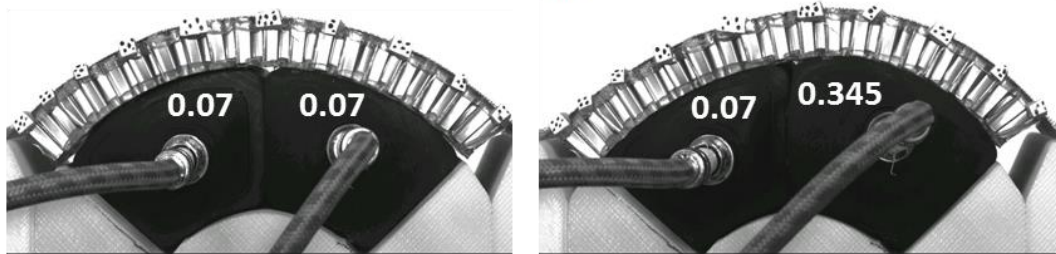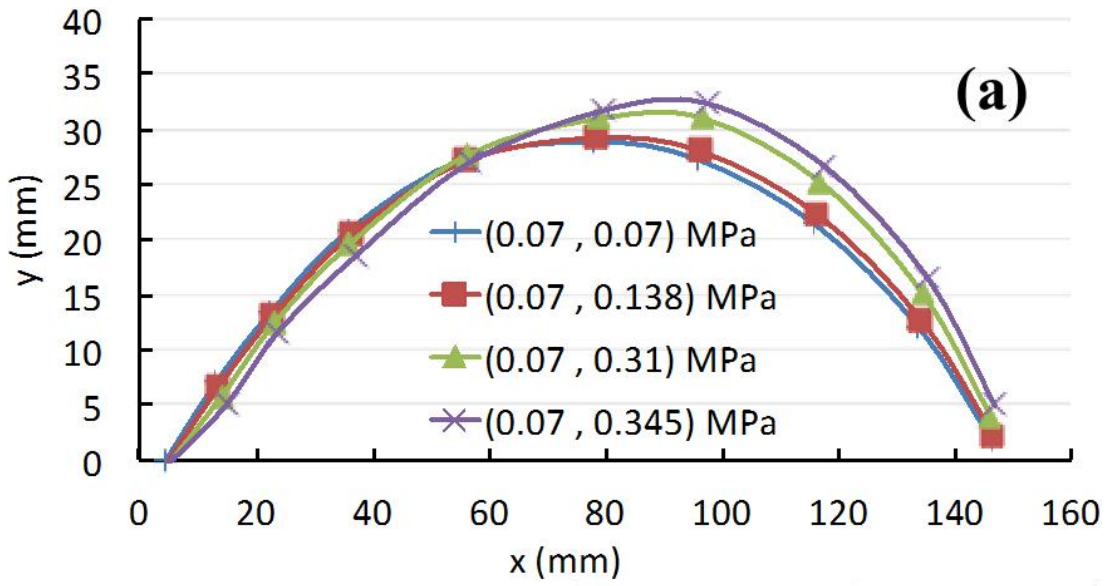
Figure 15. Shape morphing **(a)** with the right actuator inflated to higher pressures, **(b)** with the left actuator inflated to higher pressures

Table 4. % Deflection achieved for morphing from initial to end configuration

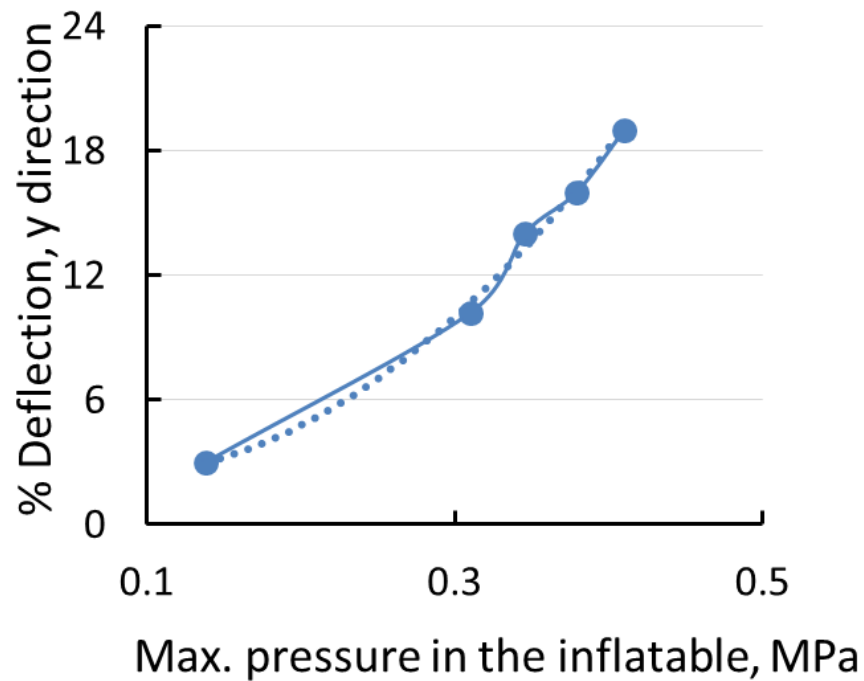| Configuration (Initial to end)	% Deflection, y direction
(0, 0) to (0.07, 0) MPa	6.5
(0.07, 0.07) to (0.07, 0.138) MPa	3
(0.07, 0.07) to (0.07, 0.31) MPa	10.2
(0.07, 0.07) to (0.07, 0.345) MPa	15
(0.07, 0.07) to (0.379, 0.07) MPa	16
(0.07 – 0.07) to (0.41 – 0.07) MPa	19

Figure 16. % Deflection vs. maximum pressure in one of the inflatables (either P_1 or P_2), all configurations start from (0.07 MPa, 0.07 MPa)

Figure 17 shows the 2D images of the external surfaces attained at various pressure contours. The graphs show the displacement in y-direction, with the red colour indicating the highest magnitude of the displacement. It is quite noticeable the fairly uniform displacement distribution along the depth of the morphing sandwich panel, although some slight edge effects (i.e., higher displacements) could be observed for the cases corresponding to the highest pressures adopted. The edge effects are also due to the effective non-zero Poisson's ratio of the Flex core honeycomb that creates an anticlastic curvature, together with the positive Poisson's ratio of the TPU skins. Overall, the results however indicate that a controllable camber change with uniform distributions along the depth of the morphing panel can be achieved through differential pressure loading.
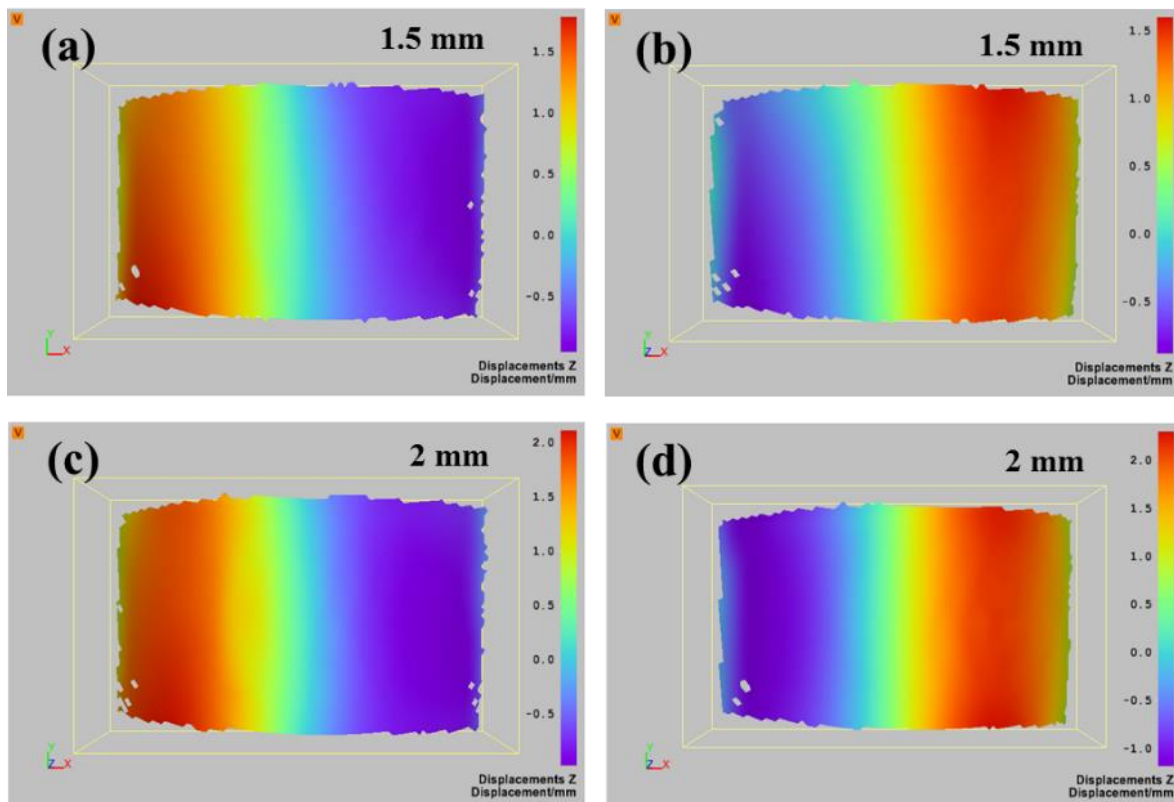

Figure 17. 2D deflection captured with 2 camera system, for configurations **(a)** (0.138 MPa, 0.0345 MPa) **(b)** (0.0345 MPa, 0.138 MPa) **(c)** (0.207 MPa, 0.0345 MPa) **(d)** (0.0345 MPa, 0.207 MPa), values denote maximum deflection in y direction

Conclusions

We have presented a concept for a morphing nacelle inlet lip based on the use of novel flexible sandwich structures and pneumatic actuators. The concept was approached from materials science perspective, taking into account critical design goals such as camber change under specific pressure distributions, lightweight characteristics and lightning strike protection. We have also proposed a novel manufacturing technique able to produce lightweight and flexible sandwich panels with high bending stiffness and out-of plane rigidity. Graphene doped thermoplastic polyurethane showed promise as face skin for the flexible morphing sandwich panels, with significantly higher bending stiffness and moderate electrical conductivity. An experimental prototype of the morphing inlet structure encompassing the flexible sandwich panel as the outer smooth aerodynamic surface and pneumatic actuators underneath was built and tested. Smooth contours with a maximum of 20% deflection were achieved at various morphing configurations, showing the feasibility of further exploring this flexible sandwich panel concept as a promising solution for morphing aerospace nacelle structures.

References

[1] S. Barbarino, "A Review of Morphing Aircraft," *JOURNAL OF INTELLIGENT MATERIAL SYSTEMS AND STRUCTURES,* vol. 22, pp. 823-55, 2011.

[2] G. R. Andersen, "Aeroelastic Modeling, Analysis and Testing of a Morphing wing structure," in *48th AIAA/ASME/ASCE/AHS/ASC Structures, Structural Dynamics, and Materials Conference*, Hawaii, 2007.

[3] J. N. Kudva, "Overview of the DARPA smart wing project," *Journal of intelligent material systems and structures,* vol. 15, pp. 261-8, 2004.

[4] Y. Chen and W. Yin, "Structural design and analysis of morphing skin embedded with pneumatic muscle fibres," *Smart Mater. Struct.,* vol. 20, 2011.

[5] Y. J. Chen, F. Scarpa, I. Farrow, Y. Liu and J. Leng, "Composite flexible skin with large negative Poisson's ratio range: numerical and experimental analysis," *Smart materials and structures,* vol. 22, 2013.

[6] J. Sun, H. Gao, F. Scarpa, C. Lira, Y. Liu and J. Leng, "Active inflatable auxetic honeycomb structural concept for morphing wingtips," *Smart Materials and Structures,* vol. 23, 2014.

[7] J. Sun, F. Scarpa, Y. Liu and J. Leng, "Morphing thickness in airfoils using pneumatic flexible tubes and Kirigami honeycomb," *Journal of intelligent material systems and structures,* pp. 1-9, 2015.

[8] R. D. Vocke, C. S. Kothera, A. Chaudhuri, B. K. Woods and N. M. Wereley, "Design and testing of a high-specific work actuator using miniature pneumatic artificial muscles," *Journal of intelligent material systems and structures,* vol. 23, no. 3, p. 365–378, 2011.

[9] B. K. Woods, M. F. Gentry, C. S. Kothera and N. M. Wereley, "Fatigue life testing of swaged pneumatic artificial muscles as actuators for aerospace applications," *Journal of intelligent material systems and structures,* vol. 23, no. 3, p. 327–343, 2011.

[10] W. Yang and V. R. Sherman, "On the tear resistance of skin," *Nature communications,* 2015.

[11] K. R. Olympio and F. Gandhi, "Design of a Flexible Skin for a Shear Morphing Wing," *Journal of intelligent material systems and structures,* vol. 21, pp. 1755-16, 2010.

[12] S. Kota, R. Osborn, G. Ervin and D. Maric, "Mission Adaptive Compliant Wing – Design, Fabrication and Flight Test," NATO OTAN, Dayton, OH, USA.

[13] E. A. Bubert and B. K. Woods, "Design and Fabrication of a Passive 1D Morphing Aircraft Skin," *journal of Intelligent systems and structures,* vol. 21, pp. 1699-19, 2010.

[14] R. O. Kingnide and F. Gandhi, "Flexible Skins for Morphing Aircraft Using Cellular Honeycomb Cores," *Journal of intelligent material systems and structures,* vol. 21, pp. 1719-17 , 2010.

[15] R. M. Neville, A. Monti, K. Hazra, F. Scarpa, C. Remillat and I. Farrow, "Transverse stiffness and strength of Kirigami zero-v PEEK honeycombs," *Composite structures,* vol. 114, pp. 30-49, 2014.

[16] Y. Chen, F. Scarpa, C. Remillat, I. Farrow, Y. Liu and J. Leng, "Curved Kirigami SILICOMB cellular structures with zero Poisson's ratio for large deformations and morphing," *Journal of intelligent materials and structures,* pp. 1-13, 2013.

[17] A. Bezazi, F. Scarpa and R. Chrystel, "A novel centresymmetric honeycomb composite structure," *Composite structures,* vol. 71, p. 356–364, 2005.

[18] C. Lira, F. Scarpa, Y. H. Tai and J. R. Yates, "Transverse shear modulus of SILICOMB cellular structures," *Composites Science and Technology,* vol. 71, p. 1236–1241, 2011.

[19] Y. Hou, R. Neville, F. Scarpa, C. Remillat, B. Gu and M. Ruzzene, "Graded conventional-auxetic Kirigami sandwich structures: flatwise compression and edgewise loading," *Composites Part B,* vol. 59, pp. 33-42, 2014.

[20] R. Wu, J. Sun, C. Zhizhong, R. Bai and J. Leng, "Elastic composite skin for a pure shear morphing wing structures," *Journal of intelligent material systems and structures,* vol. 26, no. 3, p. 352–363, 2014.

[21] W. Zhao, "Functionalized MWNT-Doped Thermoplastic Polyurethane Nanocomposites for Aerospace coating applications," *Macromolecular materials and engineering,* vol. 295, p. 838–845, 2010.

[22] H. Kim, "Graphene/Polyurethane Nanocomposites for Improved Gas Barrier and Electrical Conductivity," *Chemistry of materials,* vol. 22, p. 3441–3450, 2010.

[23] S. Stankovich, D. A. Dikin, G. H. Dommett, K. M. Kohlhaas, E. J. Zimney, E. A. Stach, R. Piner, S. Nguyen and R. S. Ruoff, "Graphene-based composite materials," *Nature letters,* vol. 442, pp. 283-286, 2006.

[24] R. K. Paton, "Scalable production of large quantities of defect-free few-layer graphene by shear exfoliation in liquids," *Nature materials,* vol. 13, pp. 624-630, 2014.

[25] H. Kim, "Graphene/ Polymer nanocomposites," *Macromolecules,* vol. 43, p. 6515–6530, 2010.

[26] K. H. Liao, "Aquaeous reduced graphene/ thermoplastic polyurethane nanocomposites," *Polymer,* vol. 54, pp. 4555-4559, 2013.

[27] O. M. Istrate, K. R. Paton, U. Khan, A. O'Neill, A. P. Bell and J. Coleman, "Reinforcement in melt-processed polymer–graphene composites at extremely low graphene loading level," *Carbon,* vol. 78, p. 243–249, 2014.

[28] L. D. Rocha-Schmidt, A. Hermanutz, H. Baier, A. Seitz, J. Bijewitz, A. Isikveren, F. Scarpa, G. Allegri, E. Feuilloley, C. Remillat and F. Majic, "Progress towards adaptive aircraft engine nacelles," in *29th congress of the international council of the aeronautical sciences*, St. Petersburg, 2014.

[29] A. Hermanutz, L. D. Rocha-Schmidt and H. Baier, "Technology Investigation of Morphing Inlet Lip Concepts for Flight Propulsion Nacelles," in *6TH EUROPEAN CONFERENCE FOR AERONAUTICS AND SPACE SCIENCES (EUCASS)*, 2015.

[30] R. S. Lakes, "Design considerations for negative Poisson's ratio materials," *ASME Journal of mechanical design,* vol. 115, pp. 696-700, 1996.

[31] P. Achilles, "Design of sandwich structures," Robinson college, Cambridge, Cambridge, 1999.

[32] J. Qiu, "Smart skin and actuators for morphing structures," *Procedia IUTAM,* vol. 10, p. 427 – 441, 2014.

[33] A. I. S. Neves, T. H. Bointon, L. V. Melo, S. Russo, I. d. Schrijver, M. F. Craciun and H. Alves, "Transparent conductive graphene textile fibres," *Scientific reports,* vol. 5, no. 9866, pp. 1-7, 2015.

[34] L. Gong, R. J. Young and I. A. Kinloch, "Optimizing the reinforcement of polymer-based nanocomposites by graphene," *ACS Nano,* vol. 6, no. 3, pp. 2086-2095, 2012.

[35] H. Shioya, M. F. Craciun, S. Russo, M. Yamamoto and S. Tarucha, "Straining Graphene Using Thin Film Shrinkage Methods," *Nano Letters,* vol. 14, no. 3, p. 1158–1163, 2014.

[36] H. J. Qi and M. C. Boyce, "Stress strain behaviour of thermoplastic polyurethane,"

Colarado, 2004.

[37] Y. R. Lee, A. V. Raghu, H. M. Jeong and B. K. Kim, "Properties of waterborne polyurethane/functionalized graphene sheet nanocomposites prepared by an in situ method," *Macromolecular Chemistry and Physics,* vol. 210, no. 15, pp. 1247-1254, 2010.

[38] U. Khan, P. May, A. O'Neill and J. N. Coleman, "Development of stiff, strong, yet tough composites by the addition of solvent exfoliated graphene to polyurethane," *Carbon,* vol. 48, no. 14, p. 4035–4041, 2010.

[39] J. R. Potts, D. R. Dreyer, C. W. Bielawski and R. S. Ruoff, "Graphene-based polymer nanocomposites," *Polymer,* vol. 52, pp. 5-25, 2011.

[40] S. Wu, "Aligning Graphene Nanoplatelets with an External Electric Field to Improve Multifunctional Properties of Epoxy Nanocomposites," *Carbon,* vol. 94, pp. 607-618, 2015.

[41] B. Galindo, "Effect of the number of layers of graphene on the electrical properties of TPU polymers," in *2nd International Conference on Structural Nano Composites (NANOSTRUC 2014)*, 2014.